Installation and Performance Characteristics of High Capacity Helical Piles in Cohesionless Soils

Mohammed Sakr, PhD., P.Eng., Geotechnical Core Service Manager, Worley Parsons Canada Infrastructure and Environment, Edmonton, Alberta, Canada; mohammed.sakr@worleyparsons.com

ABSTRACT

The use of helical piles as a deep foundation option has considerably increased in the recent years to support a variety of loads, from small loads for several applications such as residential housing, solar farms, utilities and retrofit projects, to large loads for many applications such as commercial, power transmission lines, oil facilities and industrial applications. Therefore, it is necessary to qualify and quantify their axial capacities and performance characteristics. This paper presents the first full-scale axial compression and tension (uplift) testing program executed on large capacity helical piles installed in cohesionless soils. A total of eleven pile load tests using either single or double-helix piles with shaft diameters that varied between 324 mm to 508 mm (12¾ in to 20 in) were carried out, including seven axial compression tests and four tension (uplift) tests. The results of the axial compressive and tensile pile load tests as well as field monitoring data of helical piles installed in dense sand are presented in this paper. Based on the results of this study it was found that helical piles have developed significant resistance to axial compressive loads up to about 2920 kN (656 kips) and tensile loads up to 2900 kN (652 kips).

INTRODUCTION

Helical (screw) piles, installed by applying torque at the pile head, are an old type of foundation that was widely used in many countries before the advent of reinforced concrete piles (Kurian and Shah, 2009). It is believed that helical piles were originally invented by Alexander Mitchell in 1833 and were originally patented in London, UK (Perko, 2009). However, their application was limited to soft soil conditions since installation was performed manually and required significant time and effort. The increased popularity of the helical piling system in recent years is attributed to the combination of the development of powerful hydraulic rotary heads and the recognition of helical piles as a viable foundation option. For example, torque motors used commonly for helical pile installation up to about 2005 produced a torque of 4500 to 80,000 ft-lb (6.1 to 108.5 kN.m) while new generation of torque motors that became available on the market in the late first decade of the 2000's offer torque up to 250,000 ft-lb (339 kN.m). Helical piles offer several construction and performance advantages over conventional foundations such as cast-in-place concrete piles or driven steel piles. From a construction perspective, the main advantages of helical piles include their ease of installation using relatively small equipment, the rapid speed of installation, their suitability for construction in very limited access conditions, as well as the fact that they are removable and reusable. Likewise, in the case of high ground water level, helical piles save dewatering and/or pumping of the construction site (Bobbitt and Clemence, 1987). From a performance point of view, helical piles provide high compressive and uplift capacities (about three to five times that of traditional driven steel piles with the same shaft diameter and length, Sakr *et al* 2009). Moreover, they allow immediate loading upon installation. Also, for the case of recently filled soils where negative skin friction is considerable, the use of helical piles with smaller shaft diameters provide a viable solution in terms of reducing down drag forces and optimizing design.

The axial capacities of helical piles may be estimated analytically using either the individual bearing or cylindrical shear methods. The individual bearing method (Meyerhof and Adams 1968; Vesic 1971; and CFEM 2006) assumes that bearing failure occurs at each individual helix. The cylindrical shear method (Vesic 1971; Mitsch and Clemence 1985; Das 1990; Zhang 1999) assumes that a cylindrical shear failure surface, connecting the uppermost and lowermost helices, is formed and its axial capacity is the sum of shear resistance along the cylindrical

surface, bearing resistance above the top helix (for uplift loading) and the bearing resistance below the bottom helix (for compression loading) as well as, adhesion along the top portion of the steel shaft above the helix level.

Several numerical analyses have been carried out to investigate the axial behaviour of helical piles (or circular anchors) such as Tagaya *et al* (1983, 1988), Sakai and Tanaka (1998), Merifield *et al* (2006), and Kurian and Shah (2009). Tagaya *et al* (1983, 1988) carried out two dimensional finite element analysis assuming plane strain and axisymmetric conditions for rectangular and circular anchors and using the constitutive law of Lade and Duncan (1975). Scale effects for shallow circular anchors in dense sand were estimated by Sakai and Tanaka (1998) using a constitutive model of non-associated strain-hardening-softening elasto-plastic material. Merifield *et al* (2006) investigated the effect of the anchor shape on the uplift capacity of circular and rectangular anchors using a three-dimensional finite element formulation. They concluded that the circular shape of anchors provide higher uplift resistance compared to the square anchor. Kurian and Shah (2009) carried out a study on the behaviour of screw piles using a finite element analysis. They also carried out a parametric study using different shapes of helixes.

Helical piles may be classified depending on the size of the shaft or the installation torque into low capacity and high capacity helical piles. Low capacity helical pile may be defined as helical pile with a shaft diameter up to 178 mm (7 in) or a helical pile installed with torque less than 50,000 ft-lb (67.8 kN.m) while high capacity helical piles may be defined as helical piles with shaft diameter larger than 178 mm (7 in) or installed with torque in excess of 50,000 ft-lb (67.8 kN.m). The main objective of the present study is to evaluate the axial capacities of high performance helical piles installed in dense to very dense sand based on the results of full-scale loading tests. The specific objectives of the tests program were: (1) to evaluate installability of helical piles in dense to very dense soils; (2) to define appropriate failure criterion for large diameter helical piles, (3) to estimate their axial compressive and tensile capacities, (4) to compare their axial compressive and tensile capacities and (5) to validate design methodology for high performance helical piles. In order to achieve these objectives a total of eleven full-scale load tests were carried out including seven axial compressive tests and four axial tensile (uplift) tests. Details of the testing program are described in the next sections.

GEOTECHNICAL CONDITIONS

The testing site is located in northern Alberta, Canada. The testing site is a large site with variable soil conditions. Four different test locations were selected to represent dense to very dense sand (i.e. cohesionless material). The ground surface at the test locations was flat lying. Subsurface soil stratigraphy and ground water conditions at each location are described in detail in the following sections. It should be noted that geotechnical investigation was performed at each test location and either Standard Penetration Testing (SPT) or Cone Penetration Testing (CPT) was performed.

Soil Stratigraphy

A summary of soil stratigraphy at testing Site 1 to 4 is presented in Table 1. Soil properties were estimated based on either cone penetration testing with pore pressure measurements (CPTU) or standard penetration tests (SPT). The results from both types of testing are presented in Table 1. It should be noted that CPTU testing provides near continuous soil data while SPT provides information at specific depths (typically 1.5 m or 5 ft intervals).

Soil stratigraphy at test Site 1 consists of surface silt, sand and clay till layers that extend to a depth that varied between about 1.1 m (3.6 ft) and 1.4 m (4.6 ft) underlain by a medium dense to very dense sand layer that extended to depth of about 33 m (108 ft). The upper sand layer that extended to depth of about 11.4 m (37.4 ft) was medium dense to dense while sand below that depth was found to be dense to very dense. The sand was medium grained and contained lenses of silt. Standard penetration test (SPT) blow counts varied between 14 to 58 blows per 300 mm (1 foot) of penetration for the upper sand layer indicating a medium to very dense sand state while SPT blow counts for the lower sand layer varied between 45 and 92 blows per 300 mm (1 foot) of penetration indicating dense to very dense state. Groundwater level at the test hole location was relatively shallow and was about 3.6 m (11.8 ft) below existing ground surface.

[TABLE 1] Summary of Soil Properties

Depth m (ft)	Soil description	SPT blow count per 300 mm, (1 foot)	Total unit weight, kN/m³ (pcf)	Undrained Shear Strength* kPa (psf)	Frictional resistance angle, ϕ* (°)
Site 1					
0 – 11.4	Sand, medium dense to very dense	14-58	18 (114.5)	-	35**
11.4 – 33	Sand, dense to very dense	45-92	20 (127.2)	-	40**
Site 2					
0 – 2.5	Sand, dense	NA	19 (120.9)	-	33
2.5 – 3.7	Glacial Till, stiff	NA	18 (114.5)	55 (1150)	-
3.7 – 4.3	Sand, dense	NA	19 (120.9)	-	32
4.3 – 13.1	Sand, very dense	NA	19 (120.9)	-	36
Site 3					
0 – 6.7	Sand, very dense to very dense	NA	19 (120.9)	-	36
Site 4					
0 – 5.3	Sand, dense	NA	19 (120.9)	-	35
5.3 – 10.3	Glacial Till, very stiff	NA	19.5 (124.1)	125 (2600)	-
10.3 – 12.3	Sand, dense	NA	19 (120.9)	-	33

* Soil parameters estimated from CPT soundings

** Soil parameters estimated from SPT data

Soil stratigraphy at test Site 2 consisted of dense to very dense sand that extended to a depth of about 13.1 m (43 ft) below the existing ground level. Stiff glacial till lenses, 0.7 m (2.3 ft) thick were encountered at depths of about 3.5 m (11 ft) below existing ground. Groundwater level was at a depth of about 7.1 m (23.3 ft) below the existing ground surface. The groundwater level was obtained from a cone penetration test with pore pressure measurements (CPTU). During the CPTU test, penetration of the piezocone was halted at specific depths to carry out pore pressure dissipation tests. The dissipation of the pore water pressure with time was measured and recorded and the groundwater level was estimated based on the value of the excess pore water pressure and depth at which the dissipation test was performed.

Soil stratigraphy at test Site 3 consists of dense sand that extended to the end of CPTU at a depth of 6.7 m (22 ft). Groundwater level was at a depth of about 2.6 m (8.5 ft) below the existing ground surface. At test Site 4, the subsurface conditions consisted of dense sand that extended to a depth of 5.3 m (17.4 ft) underlain by very stiff glacial till to a depth of 10.3 m (33.8 ft) underlain by dense sand to the end of CPTU at a depth of 12.3 m (40.4 ft). Groundwater level was at a depth of about 1.0 m (3.3 ft) below the existing ground surface.

TEST PILE CONFIGURATION

The configurations for different piles considered for the helical pile load test program are summarized in Table 2. Fig. 1 provides typical helical pile configurations for both single and double-helix piles. Helical pile types identified by even numbers were for piles with double helixes (i.e. Type 4, 6 and 8) while piles identified with odd numbers were for piles with a single helix (i.e. Type 3, 5 and 7). All piles were round shaft type with different shaft diameters varying between 324 mm and 508 mm (12¾ in and 20 in) and helix diameters varying between 762 mm and 1016 mm (30 and 40 in). Helixes for double helix piles were spaced at either 2 or 3 times their helix diameter. Steel pipes were ASTM A500, Grade 3 steel with a yield strength of 350 MPa (50 ksi).

[TABLE 2] Summary of Pile Configurations

Pile Type	Shaft		Helixes			
	Diameter mm (inches)	Thickness mm (inches)	Diameter mm	Thickness mm	No of Helixes	Spacing Ratio (S/D_h)
3	324 (12 ¾)	9.5 (0.375)	762 (30)	25.4 (1)	1	-
4	324 (12 ¾)	9.5 (0.375)	762 (30)	25.4 (1)	2	3
5	406 (16)	9.5 (0.375)	914 (36)	25.4 (1)	1	-
6	406 (16)	9.5 (0.375)	914 (36)	25.4 (1)	2	3
7	508 (20)	9.5 (0.375)	1016 (40)	25.4 (1)	1	-
8	406 (16)	12.7 (0.5)	813 (32)	25.4 (1)	2	2

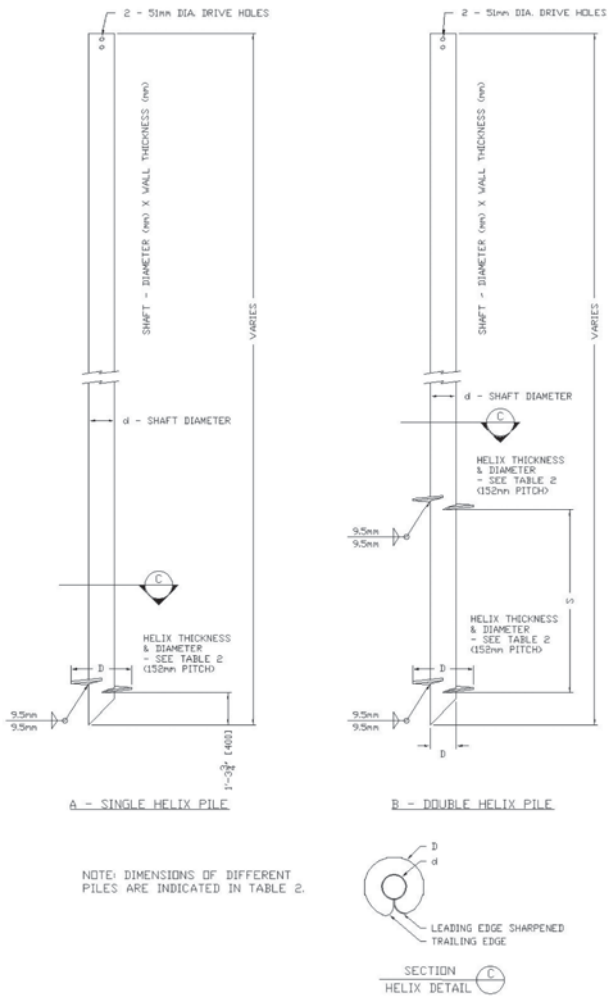

[FIG. 1] Typical Test Pile Configurations: (a) Single Helix Pile; (b) Double Helix Pile and (c) Helix Plan View

PILE INSTALLATION

Helical piles are typically installed through the use of mechanical torque applied at the pile head with a rotary hydraulic head. Fig. 2 shows a typical installation of helical piles. Table 3 provides a summary of the pile installations at all test sites; including the maximum torque recorded, predrill depth, thickness of soil plug and depth of embedment. Measured torque values were recorded at different depths for all test piles and the results are presented in Figs. 3a through 3d for piles installed at sites 1, 2, 3 and 4, respectively.

[Fig. 2] Typical Installation of Helical Piles

It can be seen from Fig. 3 (a), that for all the piles installed at Site 1, torque values increased significantly between depths of 2 and 3 m (6.7 and 10 ft) due to the presence of a hard soil layer followed by a reduction in torque values at a depth of about 4 m (13 ft). It should be noted that at test Site 1 all tested piles were predrilled using a drill auger to depths that varied between 4.0 m and 7.6 m (13 ft and 25 ft) below the existing ground surface. Upon completion of the predrilling process, the

[TABLE 3] Summary of Pile Installation

	Test ID	Pile Type	Shaft Diameter mm (inches)	Installation Torque at end of installation kN.m (ft lb)	Embedment Depth m (ft)	Soil Plug Thickness m (ft)	Predrill Depth m (ft)
Site 1	ST1	4	324 (12 ¾)	211.5 (156,000)	9.0 (29.5)	5.1 (16.7)	7.6 (24.9)
	ST2	3	324 (12 ¾)	211.5 (156,000)	9.5 (31.2)	4.1 (13.5)	6.1 (20)
	ST3	4	324 (12 ¾)	211.5 (156,000)	9.5 (31.2)	4.4 (14.4)	6.1 (20)
	ST20	5	406 (16)	338.3 (250,000)	6.1 (20.0)	3.8 (12.5)	4.5 (14.8)
	ST21	5	406 (16)	338.3 (250,000)	5.7 (18.7)	1.9 (6.2)	4.0 (13.1)
	ST22	7	508 (20)	338.3 (250,000)	5.75 (18.9)	2.9 (9.5)	4.0 (13.1)
Site 2	ST24	8	406 (16)	338.0 (250,000)	5.95 (19.5)	3.2 (10.5)	NA
	ST25	8	406 (16)	338.0 (250,000)	9.71 (31.8)	3.6 (11.8)	NA
Site 3	ST31	8	406 (16)	338.0 (250,000)	5.0 (16.4)	NA	NA
	ST32	8	406 (16)	338.0 (250,000)	5.0 (16.4)	NA	NA
Site 4	ST41	8	406 (16)	326.0 (240,400)	10.5 (34.4)	NA	NA

depths of open holes were measured and varied between 1.6 m to 3.5 m (5.1 ft and 11.5 ft) due to sloughing of sand material. The effect of the predrilling process can explain the discrepancy of torque measurements at site 1(Fig 3a). The measured torque values at end of installation for piles ST1, ST2 and ST3 (Types 3 and 4) were at 211 kN.m (156,000 ft lb). The predrill depth for pile ST1 was 7.6 m (24.9 ft.) and for piles ST2 and ST3 the depth was 6.1 m (20 ft). Pile ST1 was installed to an embedment depth of 9.0 m (30 ft), while piles ST2 and ST3 were both installed to depths of 9.5 m (31.2 ft). The measured maximum torque at the end of the installation for piles ST20, ST21 and ST22 (Type 5 and Type 7) was 338 kN.m (250,000 ft lb). The predrill depth for pile ST20 was 4.5 m (15 ft) and for piles ST21 and ST22 it was 4.0 m (13 ft).

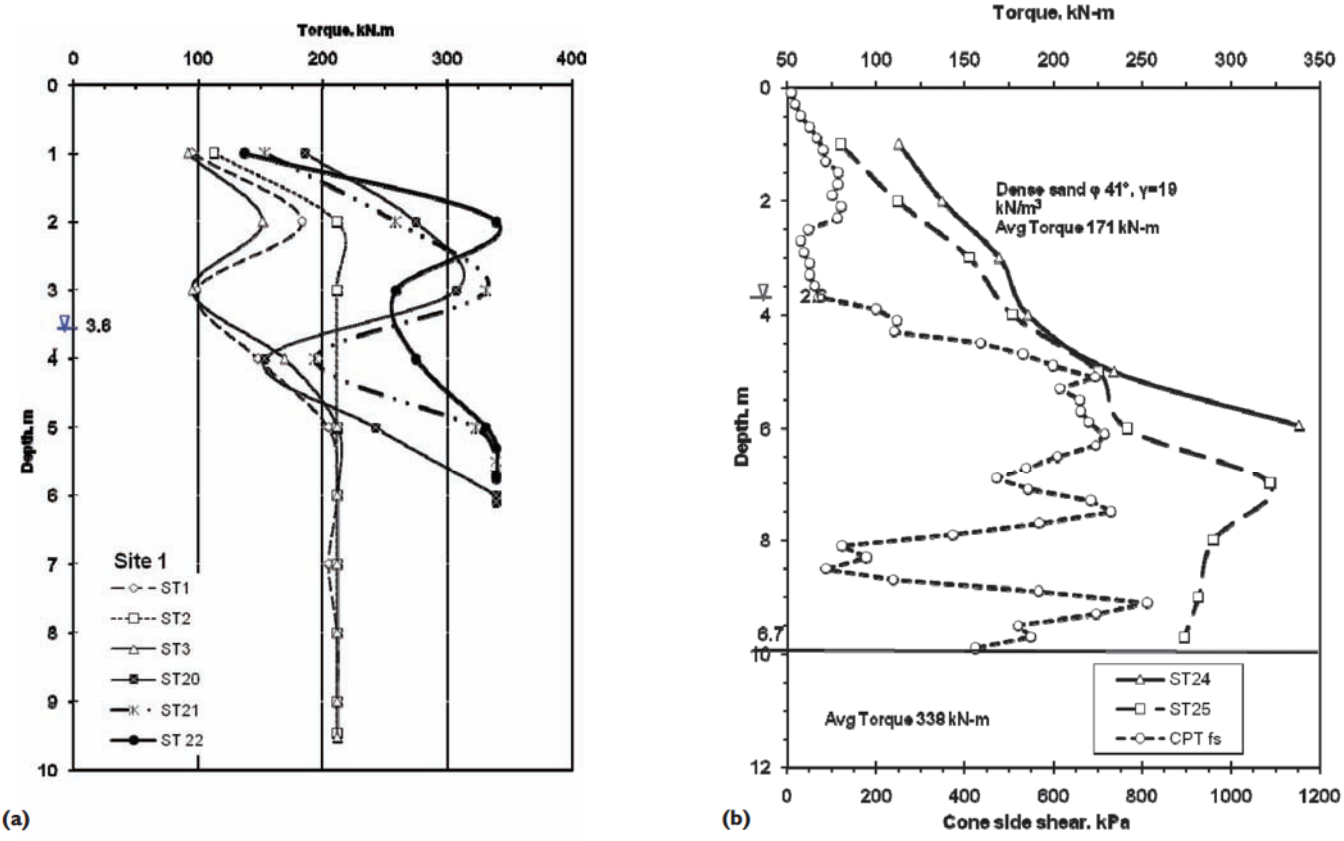

[FIG. 3] Measured Installation Torque vs. Depth for: (a) Site 1; (b) Site 2

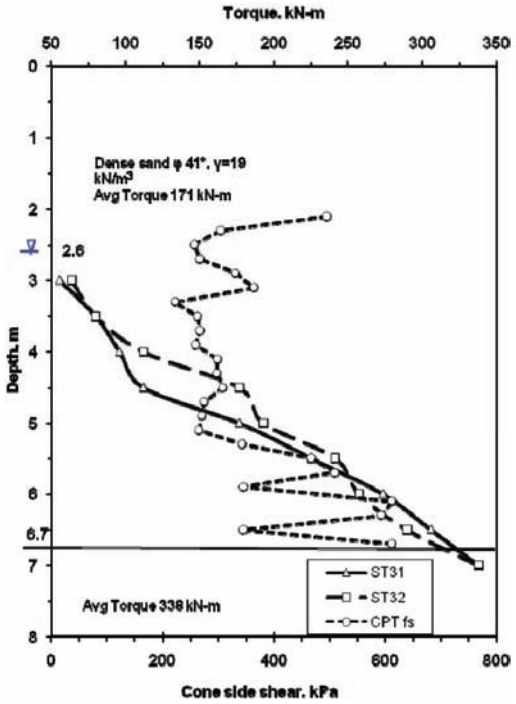

(c)

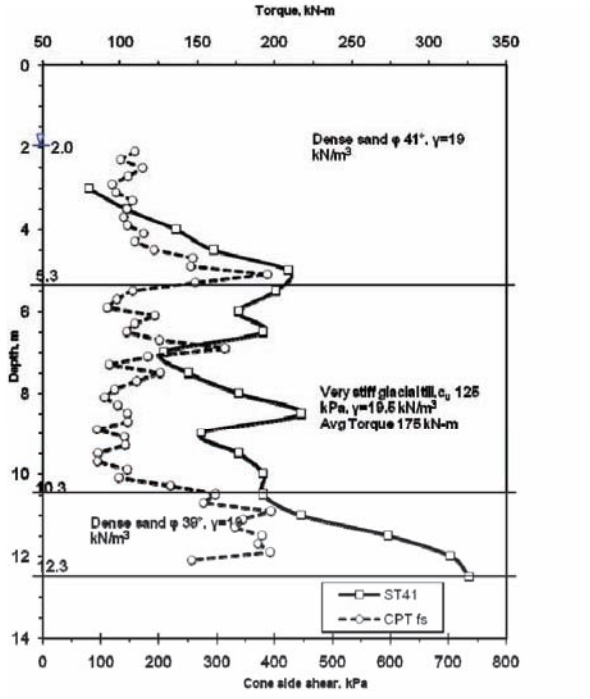

(d)

[FIG. 3] Measured Installation Torque vs. Depth for: (c) Site 3; and (d) Site 4

Pile ST20 had an embedment depth of about 6.1 m (20 ft) while piles ST21 and ST22 were embedded to a depth of about 5.7 m (19 ft).

At test Site 2 (Fig. 3b) torque values increased with depth until the end of installation. The measured maximum torque at the end of installation for pile ST24 was 338 kN.m (250,000 ft lb) and the corresponding pile embedment depth was 5.95 m (19.5 ft). It can be seen from Fig 3b that a significant increase in torque values for pile ST24 was observed between depths of about 4 and 6 m (13 ft and 20 ft). For pile ST25, torque was increased to a maximum value of 322 kN.m (237,400 ft lb) at a depth of about 7 m (23 ft) followed by a reduction in torque values. The maximum torque at the end of installation for pile ST25 was 273 kN.m (201,700 ft lb) and the corresponding pile embedment depth was 9.7 m (31.9 ft).

Test sites 3 and 4 were both excavated to about 2 m (6.7 ft) below existing ground surface prior to pile installation. Piles installed at both sites were Type 8 with double helixes spaced at two times the helix diameter. Both helixes of piles ST31, ST32 and ST41 were trimmed to facilitate pile installation into gravelly materials that contained cobbles. Trimming the helix involved cutting portions of the leading edge of the helix (about 7% to 8% of its surface area). Trimmed helixes, shown in Fig. 4, improved the ability of helical piles to displace cobbles during installation.

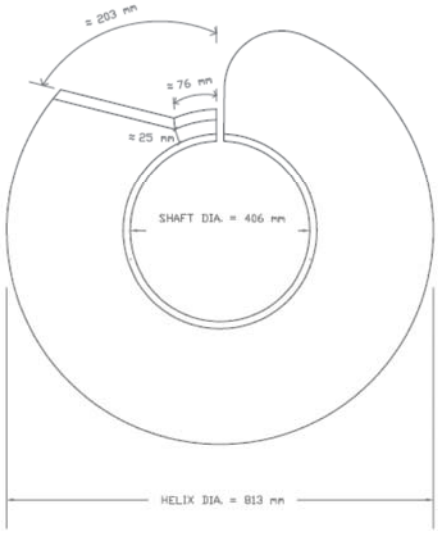

(a)

(b)

[FIG. 4] Details of Trimmed Helixes for Piles ST31, ST32 and ST41: (a) Plan View, and (b) Oblique View

It can be seen from Fig. 3c that for piles ST31 and ST32 torque values increased with depth for both piles until the end of the pile installation. The torque values between depths of 4.5 m and 7.0 m (15 and 23 ft) increased at an average rate of 75 kN.m/m and 80 kN.m/m (16.9 kip ft/ft to 18 kip ft/ft) for piles ST31 and ST32, respectively. The measured torque values at the end of installation for piles ST31 and ST32 were 338 kN.m (250,000 ft lb) and the corresponding pile embedment depth was 5.0 m (16.4 ft). Torque values versus embedment depth for pile ST41 is plotted in Figure 3d. It can be seen from Fig. 3d, that the torque values in the upper sand layer between depths of about 2.5 m and 4.5 m (8.2 and 14.8 ft) increased almost linearly with depth. For the glacial till layer between depths of 5.3 m and 10.3 m (17.4 and 33.8 ft), torque values fluctuated and did not show a clear trend. This behaviour is typical for glacial till since it typically contains lenses of silt, silty clay and clay silt material with variable consistencies. The average torque values for glacial till layer was about 175 kN.m (129 kip ft). For the lower sand layer, considerable increase in the torque values was observed between depths of about 10.3 m and 12.5 m (33.8 ft and 41 ft). The measured torque at the end of installation for pile ST41 was 326 kN.m (240 kip ft) and the corresponding pile embedment depth was 10.5 m (34.4 ft).

Sleeve friction (skin friction) measured from CPTU soundings at test sites 2, 3 and 4 are also plotted in Figs. 3b to 3d. It can be seen from these Figs. that the measured torque values generally followed a similar trend to the sleeve friction values. This observation is valuable at locations where geotechnical information is not available and design may rely on torque measurements and installation feedback. Therefore, torque monitoring during installation can provide a tool for estimating the relative consistency of soil layers since torque values tend to increase in hard soil materials and reduce in softer soil materials.

TEST SET-UP

The axial compression and tension load tests were carried out in accordance with ASTM standards D 1143-07 and D 3689-07. Since the main objective of the load tests was to determine the ultimate bearing capacity of the pile, Procedure A (Quick Test) was adopted for ten of the tests, wherein numerous small load increments were applied and maintained constant over short period of time intervals. Procedure B (Maintained Test) or slow test was used for one of the compression tests to provide a basis for comparison between both test methods and to evaluate the creep effect on the axial load test results. Seven axial compression pile load tests were carried out at all test sites. Four axial tension (uplift) tests were performed using Procedure A (Quick Test).

Setup for Axial Compressive and Tensile Load Tests

Fig. 5 shows typical load test setup using six reaction piles. Each axial compression or tension test setup included a total of seven piles including the test pile and six reaction piles. The arrangements for applying loads to the test piles involved the use of a hydraulic jack acting against the test beam. The axial loads were applied at the pile head using two 1800 kN (200 ton) hydraulic jacks situated at the pile head for the case of compression test. For the case of tension tests, the hydraulic jacks were placed on the top of the test beam and the test pile was connected to the load cell through a loading frame consisting of four 50.8 mm (2 in) diameter all-thread Grade 8 steel Dywidag bar and a 51 mm (2 in) thick steel plate. The load at the pile head was measured using a 7400 kN (1650 kips) strain gauge load cell that was calibrated up to 4500 kN (1000 kips). A redundant hydraulic pressure transducer (10,000 psi or 69 MPa capacity and 0.25% FS accuracy) was also attached to the hydraulic jack to measure the pressure applied at the pile head. Pile head axial movements were monitored at four points during the test, using two independently supported Linear Displacement Transducers (LDT) (0.05 mm accuracy (0.01 in) - 150 mm (6 in) travel) and two mechanical dial gauges (0.05 mm (0.01 in) accuracy - 50 mm (2 in) travel). The LDTs were oriented in orthogonal directions so their stems were perpendicular to the vertical axis of the test pile cap and were bearing against a glass plate affixed to the pile cap. All of the LDTs, load cell and pressure transducer readings were recorded automatically using a Flex Data Logger system at intervals of 30-seconds throughout the duration of the test.

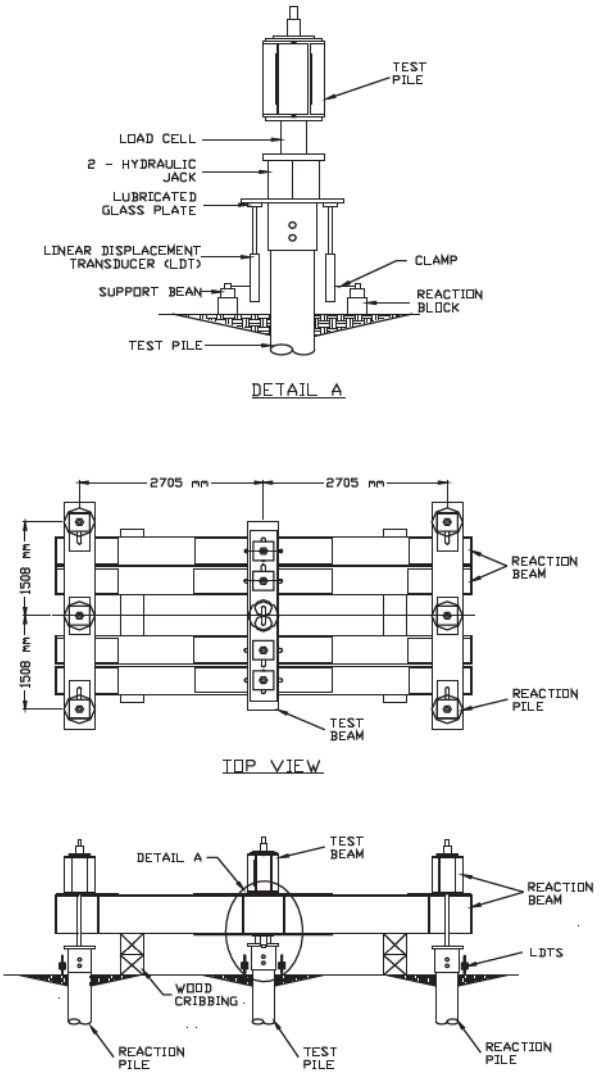

(a)

(b)

[FIG. 5] Axial Compression Load Test Setup: (a) Schematic View, and (b) Oblique View for Test Setup using Six Reaction Piles

Test Procedures for Axial Load tests (Compression and Uplift)

The following specific test procedures using Procedure A for Quick Tests for piles under axial compressive or uplift loads were applied:

1. Apply test loads in increments equal to 5% of the anticipated failure loads and maintained load constant for 5 minutes. Monitor movements using LDTs at intervals of 30 seconds. Monitor movements using mechanical dial gauges at the beginning and at the end of each load increment.
2. Add load increments until reaching a failure load but do not exceed the safe structural capacity of the pile or reaction apparatus. When reaching the failure load, maintain the load for a longer period of time to monitor creep behaviour (about 10 to 15 minutes).
3. Unload test pile in five increments and hold for 5 minutes with same monitoring intervals as for loading. When reaching zero loads continue monitoring the LDTs readings for 10 minutes to assess the rebound behaviour.

TEST RESULTS

Axial Compressive Load Test Results

The load displacement curves (Figs. 6 and 7) are used to determine the axial compressive load capacities of the piles tested at sites 1 to 4. The load displacement curves for test piles ST1, ST2, ST21, ST22 tested at Site 1 are presented in Fig. 6 while the load displacement curves for piles ST24, ST31 and ST41 tested at Sites 2 to 4 are presented in Fig. 7. In general the load displacement curves can be characterized into three parts: the first linear part up to a displacement of about 2 mm (0.08 in), followed by a nonlinear component that continued up to displacements that varied between about 25 mm and 45 mm (1.0 and 1.8 in) followed by a secondary linear component with less slope. No plunging failure was observed for any pile tested and piles continued to resist higher loads up to the end of testing. The applied loads at the pile head at the end of initial linear component varied between about 280 kN (62.9 kips) for Pile ST1 and about 500 kN (112.4 kips) for pile ST24. When comparing between the load-displacement curves for piles ST1 with double 762 mm (30 in) helixes and pile ST2 with a single 762 mm (30 in) helix, the data showed that both piles had a similar performance. This observation contradicted the fact that piles with double helixes generally provide a stiffer response at high displacement levels; i.e. higher loads at the same displacement levels (Sakr, 2009). This odd behavior can be explained by

the deep predrilling process used for pile ST1 to depth of 7.6 m (25 ft), which is deeper than the depth to the upper helix, which resulted in disturbing the bearing soil layer at the upper helix level, and losing considerable component of the skin friction along the pile shaft.

It should be noted that piles ST24, ST31 and ST41 were Type 8 with shaft diameter of 406 mm (16 in), double helixes of 813 mm (32 in) in diameter, and spaced at two times the helix diameter; but they had different embedment depths as per Table 3. Comparing between load displacement curves for pile ST24 with an embedment depth of 5.95 m (19.5 ft) and pile ST31 with an embedment depth of 5 m (16.4 ft), as well as the same configurations, (Fig. 7) indicates that pile ST31 exhibited a softer response that manifested in lower loads at the same displacement levels. This behavior can be explained by the fact that both helixes for pile ST31 were trimmed and therefore the bearing area was reduced which resulted in reducing its compressive resistance.

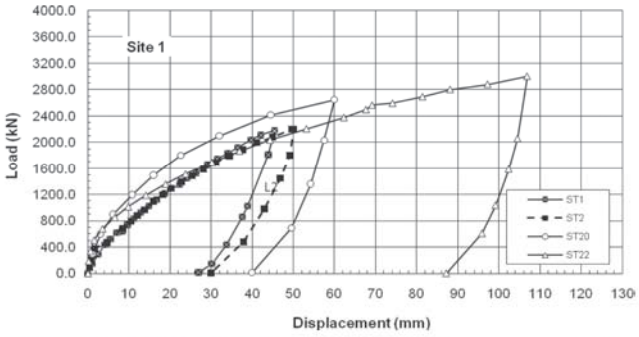

[FIG. 6] Applied Loads at Pile Head vs. Displacement for Axial Compression Pile Load Tests for Pile ST1, St2, ST20 and ST22

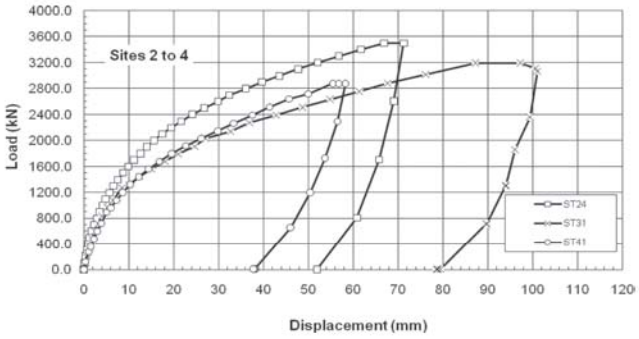

[FIG. 7] Applied Load at Pile Head vs. Displacement for Axial Compression Pile Load Tests at Sites 2 to 4 for Pile ST24, St31, and ST41

Axial Compressive Capacity

There are a large number of failure criteria used to interpret the axial compressive capacities of piles from pile load test results such as the Davisson criterion, Brinch Hansen, L1-L2 method, FHWA (5%) and ISSMFE (10%). Davisson's criterion (1972) is the most widely used method for estimating the axial capacities of piles. In Davisson's criterion the ultimate capacity is defined as the load corresponding to a total displacement equal to the sum of elastic deflection of the pile $\left(\frac{PL}{AE}\right)$ and the offset as identified in Equation [1] below:

$$S = \frac{PL}{AE} + \frac{d}{120} + 4(mm) \qquad [1]$$

where S = the displacement in mm;

P = load on pile;

L = pile length in m;

A = cross sectional area;

E = Young's modulus of pile material; and

d = pile diameter in mm.

It is worth mentioning that the Davisson criterion was initially developed for driven steel piles with small diameters up to 305 mm (12 in). The main shortcoming of applying Davisson's criterion for helical piles is that the offset limit was initially developed to satisfy the movements necessary to mobilize toe resistance of driven steel piles with small toe diameter. Davisson (1993) suggested that for drilled shaft piles the term that contains diameter, d, to be multiplied by a factor of 2 to 6. Nesmith and Siegel (2009) and Kulhawy and Hirany (2009) argued the use of the Davisson criterion with large diameter cast-in-place concrete piles. It should be noted that helical piles derive most of their resistance from the helixes and end bearing component and therefore, the use of Davisson criterion is likely to yield lower capacities that do not reflect the actual capacities of helical piles.

Hirany and Kulhaway (1989) developed L1-L2 failure criterion for load displacement curves that exhibit three regions similar to the load test results of all piles considered in this study (i.e. linear, transient and final linear components). Point L1 corresponds with the load at the end of first linear component that represents the frictional resistance of the pile and L2 is the load at the beginning of the second linear component, beyond which a small increase in load produces a significant increase in displacement.

Sakr (2009) defined the ultimate capacity of a helical pile as the load that corresponds to a displacement of 5% of the helix diameter. It should be noted that the end bearing capacity is typically fully mobilized at relatively large displacement levels (about 10%). However the 10% displacements of large diameter helical piles are relatively large. For example for a helical pile with helix diameter of 1016 mm (40 in), the displacements that produce the ultimate capacity using 10% and 5% criteria are about 102 mm (4 in) and 51 mm (2 in), respectively. Therefore, the 5% failure criterion provides a more reasonable estimate of the ultimate capacity of helical piles at practical displacement levels since in many cases, design is controlled by allowable vertical displacement.

In the present study the ultimate capacities of helical piles were estimated using the L1-L2 and 5% criterion, as well as Davisson's failure criterion. The results of these estimations are presented in Table 4. At test site 1, the ultimate capacities for piles ST1, ST2, ST20 and ST22 using 5% displacement criterion were about 2030, 1892, 2533 and 2200 kN, (456.4, 425.3, 569.4 and 494.6 kips) respectively, while the ultimate pile capacities based on L1-L2 criterion were 1680, 1650, 2100 and 1880 kN (377.7, 370.9, 472.1 and 422.6 kips), respectively. The use of L1-L2 method to estimate the ultimate capacities of different piles resulted in lower estimate than the 5% criterion by about 13% to 18%. The ultimate load capacities for tested piles using the Davisson failure criterion were 1057, 1030, 1487 and 1255 kN (237.6, 231.6, 334.3 and 282.1 kips), respectively. As expected, Davisson criterion yielded significantly lower capacities than L1- L2 and 5% criteria by up to 47% and the corresponding displacement levels were about 15 mm (0.59 in). It can also be observed from Table 4 that the axial capacity of pile ST20 with a single helix of 914 mm (36 in) in diameter was higher than that of pile ST22 with a single helix of 1016 mm (40 in) in diameter. This odd behaviour is likely due to the presence of denser sand material localized at the location of test pile ST20.

At test sites 2 to 4 (Fig. 7), the ultimate capacities for piles ST24, ST31 and ST41 (Type 8) using 5% displacement criterion were about 2920, 2320, and 2511 kN (656.4, 521.6 and 564.5 kips), respectively. The axial capacities of piles ST24, ST31 and ST41 using Davisson criterion were 1899 kN, 1460 kN, and 1600 kN (426.9, 328.2 and 359.7 kips), and the corresponding displacements were 14 mm, 13 mm and 16 mm (0.55, 0.51 and 063 in) respectively. The axial capacities of piles ST24, ST31 and ST41 using the L1-L2 criterion were 2401 kN, 2034 kN and 2031 kN (539.8,

[TABLE 4] Summary of Axial Compressive Load Test Results

Site ID	Test ID	Pile Type	Shaft Dia. mm (in)	Helix Dia. mm (in)	Ultimate Capacity (Davisson)		Ultimate Capacity L1-L2		Ultimate Capacity 5%	
					Load kN (kips)	Dispt. mm (in)	Load kN (kips)	Dispt mm (in)	Load (kN)	Dispt. mm (in)
Site 1	ST1	4	324 (12 ¾)	762 (30)	1057 (237.6)	15 (0.59)	1680 (377.7)	29 (1.14)	2030 (456.4)	38 (1.5)
	ST2	3	324 (12 ¾)	762 (30)	1030 (231.6)	14.7 (0.58)	1650 (370.9)	29 (1.14)	1892 (425.3)	38 (1.5)
	ST20	5	406 (16)	914 (36)	1487 (334.3)	15 (0.59)	2100 (472.1)	31 (1.22)	2533 (569.4)	46 (1.8)
	ST22	7	508 (20)	1016 (40)	1255 (282.5)	15 (0.59)	1880 (422.6)	37 (1.46)	2200 (494.6)	51 (2.0)
Site 2	ST24	8	406 (16)	813 (32)	1899 (426.9)	14 (0.55)	2401 (539.8)	24 (0.94)	2920 (656.4)	41 (1.6)
Site 3	ST31	8	406 (16)	813 (32)	1460 (328.2)	13 (0.51)	2034 (457.5)	27 (1.06)	2320 (521.6)	41 (1.6)
Site 4	ST41	8	406 (16)	813 (32)	1600 (359.7)	16 (0.63)	2031 (456.6)	26 (1.02)	2511 (564.5)	41 (1.6)

457.3 and 456.6 kips), and the corresponding displacements were 24, 27 and 26 mm (0.94, 1.06 and 1.02 in), respectively. The axial capacities of piles estimated using L1-L2 method were about 13% to 19% lower than that values estimated using the 5% criterion. The estimated capacities using the Davisson criterion were about 35% to 37% lower than the 5% criterion. Piles ST24 and ST31 were both Type 8, installed in similar soil conditions, and had similar embedment depths of 5.95 m and 5 m (19.5 and 16.4 ft.). The only difference is that for pile ST31, both helixes were trimmed (see Fig, 4). As expected, the trimmed helixes had resulted in reducing its bearing area and the axial capacity of pile ST31 is about 80% of ST24. The reduction in the axial capacity of pile ST31 is consistent with the reduction of its bearing area.

Evaluating Creep Effects

In order to evaluate the creep effect on the pile load test results, displacement and displacement rate versus time at load increments of 1500 kN (337 kips) (equivalent to the pile capacity using the Davisson criterion) and 2700 kN (607 kips) (final load increment which is higher than the pile capacity using the 5% criterion) were plotted for pile ST20 and the results are shown in Fig, 8. It can be seen from Fig. 8 that at load level of 1500 kN (337 kips), about 90% of the incremental displacement was obtained within 5 minutes. After five minutes the creep rate was almost steady at a rate of about 0.5 mm/hour (0.02 in/hour). The finial differential displacement at the end of the load increment was about 4.5 mm (0.18 in). At load level of 2700 kN (607 kips), about 87% of incremental displacement was obtained within 5 minutes. After a five minutes period, the creep rate was almost steady at a rate of about 1.9 mm/hour (0.07 in/hour) and the finial differential displacement at the end of load increment of 2700 kN (607 kips) was about 14.7 mm (0.58 in). This observation supports that most of the displacement at any load increment for dense to very dense sand soils is likely to occur in the first five-minute period and therefore the creep effect is minor. Therefore, the period of sustained loads after five minutes has a small effect on the load-displacement characteristics and the results of quick tests can be used to estimate the axial behaviour of cohesionless soils with a reasonable accuracy especially at low displacement levels.

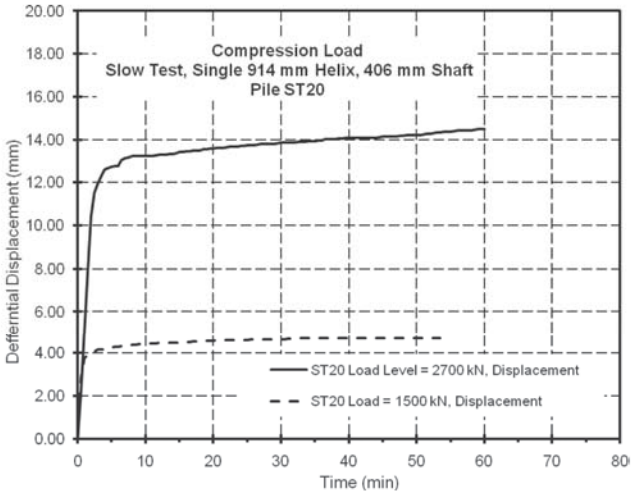

[FIG. 8] Evaluating Creep Effect at Load Levels of 1500 kN and 2700 kN (337 and 607 kips)

Axial Tensile (Uplift) Load Test Results

The results of uplift load tests performed in cohesionless soils at test sites 1 to 3 are also presented in Fig. 9 and 10 in the form of load displacement curves. These curves are used to determine the load capacities of the piles. It can be seen from Fig. 9 and 10, that similar to compression tests, the load displacement curves can be characterized into three parts: the first linear part up to a displacement of about 1 mm to 2 mm (0.04 to 0.08 in), followed by a nonlinear component up to a displacement level of about 25 mm (1.0 in) for pile ST3 and 32 mm (1.26 in) for ST21, and a secondary linear component with less slope. The loads at the pile head at the end of the initial linear component were about 150 kN and 960 kN (33.7 and 215.8 kips) for piles ST3 and ST25, respectively.

Pile ST21 was loaded to a relatively large displacement level of about 83 mm (3.3 in) to investigate the post failure behaviour. However pile ST21 continued to resist loads up to the final loading increments with no indication of plunging failure. Comparing between the load-displacement curves for both piles ST3 and ST21, indicated that the slope of the second linear component of the load displacement curve for pile ST3 with double helixes was approximately 200% steeper than that of ST21. This observation suggested again that double-helix piles perform better than single-helix piles at high displacement levels.

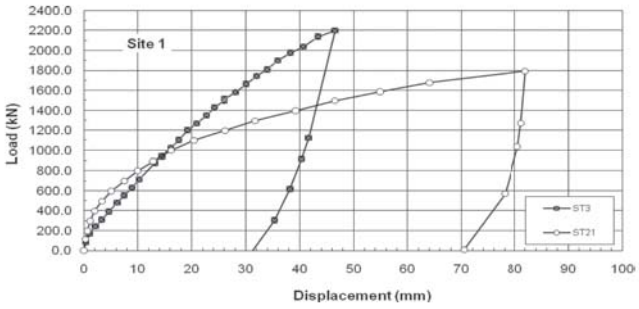

[FIG. 9] Applied Loads at Pile Head vs. Displacement for Axial Tension (Uplift) Pile Load Tests for Piles ST3 and ST21 – Site 1

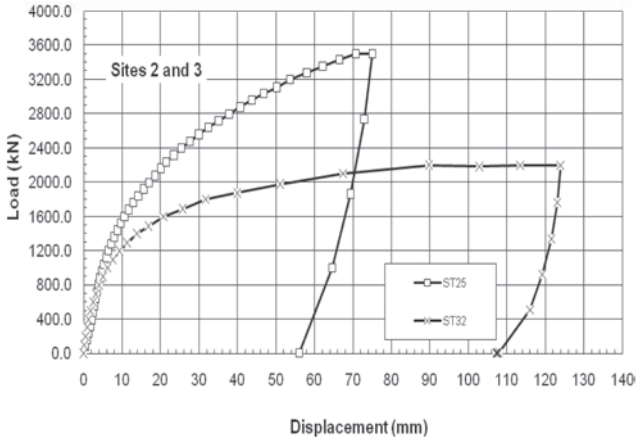

[FIG. 10] Applied Loads at Pile Head vs. Displacement for Axial Tension (Uplift) Pile Load Tests for Piles ST25 and ST32 – Sites 2 and 3

A comparison between the load displacement curves for piles ST25 and ST32, (Type 8 Fig. 10) indicates that the loads at the pile head at the end of initial linear component were about 960 kN and 500 kN (215.8 and 112.4 kips) for piles ST25 and ST32, respectively, and the corresponding displacements were about 5 mm and 2 mm (0.2 and 0.08 in). The higher frictional resistance of pile ST25 is due to its longer embedment depth (about 9.7 m or 31.8 ft) when compared to pile ST32 with an embedment depth of about 5.0 m (16.4 ft). At a high displacement level, pile ST25 showed stiffer response than pile ST32, and that manifested in steeper secondary slope of the load displacement curve. This can be attributed to the effect of trimming the leading edge of both helixes of pile ST32, which resulted in reducing its bearing area. Pile ST32 reached a plunging failure at a displacement level of about 90 mm (3.5 in) and a corresponding load of about 2200 kN (494.6 kips).

Axial Tensile Capacity

The ultimate tensile capacities of helical piles were estimated using the L1-L2, 5% criterion, as well as the Davisson failure criteria and the results are presented in Table 5. At test site 1, the ultimate capacity using the 5% criterion of pile ST3 (Type 4) with a double helix was 1993 kN (448 kips) while the uplift capacity of pile ST21 (Type 5) with a single helix was about 1493 kN (335.6 kips). The axial capacities of piles ST3 and ST21 using L1-L2 limits were about 1420 kN and 1300 kN (319.2 and 292.3 kips), which is about 30% to 10% lower than the capacities using the 5% criterion. The axial uplift capacities of piles ST3 and ST21 using Davisson's criterion were 913 kN and 990 kN (205.3 and 22.6 kips) respectively. As expected, the axial uplift capacities of piles using the Davisson criterion were considerably lower than those estimated using the 5% criterion and this corresponds to relatively low displacement levels of about 14 mm (0.55 in).

At test sites 2 and 3, the ultimate tensile capacities using the 5% criterion of piles ST25 and ST32 (Type 8) with double helixes were 2900 kN and 1880 kN (651.9 and 422.6 kips), respectively. The tensile capacities of piles ST25

[TABLE 5] Summary of Axial Tension (Uplift) Test Results

Site ID	Test ID	Pile Type	Shaft Dia. mm (in)	Helix Dia. Mm (in)	Ultimate Capacity (Davisson)		Ultimate Capacity L1-L2		Ultimate Capacity 5%	
					Load kN (kips)	Dispt. mm (in)	Load kN (kips)	Dispt mm (in)	Load kN (kips)	Dispt. mm (in)
Site 1	ST3	4	324 (12 ¾)	762 (30)	913 (205.3)	14.5 (0.57)	1420 (319.2)	24 (0.94)	1993 (448.9)	38 (1.5)
	ST21	5	406 (16)	914 (36)	990 (222.6)	14 (0.55)	1300 (292.3)	32 (1.26)	1497 (336.5)	46 (1.8)
Site 2	ST25	8	406 (16)	813 (32)	1700 (382.2)	17 (0.67)	2558 (575.1)	30 (1.18)	2900 (651.9)	41 (1.6)
Site 3	ST32	8	406 (16)	813 (32)	1350 (303.5)	13 (0.51)	1801 (404.9)	32 (1.26)	1880 (422.6)	41 (1.6)

and ST32 using L1-L2 limits were about 2558 kN and 1801 kN (575.1 and 404.9 kips), which is about 4% to 12% lower than that capacities using the 5% criterion. The axial uplift capacities of piles ST25 and ST32 using the Davisson criterion were 1700 kN and 1350 kN (382.2 and 303.5 kips) respectively. The axial uplift capacities of piles tested at sites 2 and 3 using the Davisson criterion were also considerably lower and this corresponds to a relatively low displacement levels of about 17 mm and 13 mm (0.67 and 0.51 in) for piles ST25 and ST32.

COMPARISON BETWEEN MEASURED AND ESTIMATED PILE CAPACITIES

Axial Compressive Load Test Results

The international Building Code (2009) provided a general guideline for design of helical piles. The allowable axial design load of helical piles determined from the International Building Code (2009) as half of the ultimate pile capacity using the least value of the following:

1. Sum of the areas of the helical bearing plates times the ultimate bearing capacity of the soil or rock comprising the bearing stratum.
2. Ultimate capacity determined from well-documented correlations with installation torque.
3. Ultimate capacity determined from load tests.
4. Ultimate axial capacity of pile shaft.
5. Ultimate axial capacity of pile shaft couplings.
6. Sum of the ultimate axial capacity of helical bearing plates affixed to pile.

However, the Canadian Foundation Engineering Manual (2006) provided more specific details about the determination of the ultimate capacity of helical piles. Therefore, for the cohesionless soils encountered at test sites 1 to 4, the ultimate compressive capacities of the helical piles can be estimated using the following expression (Canadian Foundation Engineering Manual, 2006):

$$R = \sum Q_h + Q_f \qquad [2]$$

where R = ultimate pile capacity;

Q_h = individual helix bearing capacity

Q_f = shaft resistance

The individual helix bearing capacity can be estimated from the following expression:

$$Q_h - A_h(\gamma D_h N_q + 0.5\gamma D N_\gamma) \qquad [3]$$

where A_h = projected helix area

γ = Unit weight of the soil;

D_h = depth to helical bearing plate

D = diameter of helical plate

N_q and $N\gamma$ = bearing capacity factors for local shear conditions.

As indicated the CFEM (2006), the shaft resistance, Q_f can be estimated from the following expression:

$$Q_f = \sum \pi d \Delta L_i q_{si} \qquad [4]$$

where d = shaft diameter

ΔL_i = length of pile segment in soil layer *i*; and

q_{si} = average unit shaft friction of soil layer i

The unit shaft friction for the cohesionless soils can be estimated using $q_{si} = \sigma_v K_s \tan(\delta)$, where σ_v is the effective vertical stress at the mid depth of each soil layer; K_s is the coefficient of lateral earth pressure ($K_s = 2(1 - \sin(\phi))$ for torque driven piles); and ϕ and δ are the frictional resistance and the interface friction angles.

The estimated axial capacities for different piles are presented in Table 6 using soil parameters in Table 1. The shaft resistance was established from the load displacement curves as the load at the end of the first linear component of the load displacement curve. In all cases the estimated shaft resistances were at displacement levels less than or equal to about 2 mm (0.08 in). The estimated capacities were also compared to the measured capacities based on the 5% criterion.

In general the estimated compressive capacities for the piles tested at site 1 agreed reasonably with the measured values with the exception of pile ST1. The axial capacity of pile ST1 was overestimated by approximately 33%. The lower measured capacity of pile ST1 is likely due to the effect of predrilling since the predrilled hole for pile ST1 was 7.5 m (24.6 ft) deep, which is deeper than the depth to the top helix. Therefore the bearing resistance of the top helix was considerably lower than the estimated value assuming no disturbance at the helix level. The measured capacity for ST20 was about 18% higher than the estimated value. A possible reason for that discrepancy is the

[TABLE 6] Comparison between Measured and Estimated Axial Compressive Capacities

Site	Test ID	Pile Type	Ultimate Capacity Estimated			Ultimate Capacity (5%) Measured			Prediction Ratio
			Shaft kN (Kips)	Helix(es) kN (Kips)	Total kN (Kips)	Shaft kN (Kips)	Helix(es) kN (Kips)	Total kN (Kips)	
Site 1	ST1	4	300 (67.4)	2396 (538.6)	2696 (606.1)	280 (62.9)	1750 (393.4)	2030 (456.3)	1.33
	ST2	3	587 (132.0)	1690 (379.9)	2277 (511.9)	400 (89.9)	1492 (335.4)	1892 (425.3)	1.2
	ST20	5	307 (69.0)	1765 (396.8)	2072 (465.8)	300 (67.4)	2233 (502.0)	2533 (569.4)	0.82
	ST22	7	323 (72.6)	2090 (469.9)	2413 (542.5)	500 (112.4)	1700 (382.2)	2200 (494.6)	1.1
Site 2	ST24	8	315 (70.8)	2756 (619.6)	3071 (690.4)	500 (112.4)	2420 (544.0)	2920 (656.4)	1.05
Site 3	ST31	8	544 (122.3)	2270 (510.3)	2814 (632.6)	360 (80.9)	1960 (440.6)	2320 (521.5)	1.21
Site 4	ST41	8	795 (178.7)	2270 (510.3)	3065 (689.0)	480 (107.9)	2030 (456.4)	2510 (564.3)	1.22

presence of a localized denser sand lens at the location of ST20 pile load test.

The estimated axial compressive capacities at test sites 2 to 4 for piles ST24, ST31 and ST41 (Type 8) were also compared to the measured capacities based on the 5% criterion and the ratio between estimated and measured axial compressive capacities were 1.05, 1.21 and 1.22, respectively. The axial capacities of piles ST31 and ST41 were overestimated since the estimated capacities did not account for the reduced bearing area due to trimming both helixes. When the reduced bearing area is considered, the estimated axial compressive capacities of piles ST31 and ST41 were 2450 kN and 2700 kN (550.8 and 607 kips), respectively and the prediction ratios were 1.06 and 1.08, respectively.

Axial Tensile (Uplift) Results

Similar to compressive loading, uplift capacities of piles tested in cohesionless soils can be estimated using Eqn. (2) where the individual helix uplift capacity, Qh can be estimated using Eqn. (5) (Das 1990) listed below.

$$Q_h = A_h \gamma D_h F_q \qquad [5]$$

where A_h = projected helix area

γ = Unit weight of the soil;

D_h = depth to helical bearing plate

F_q = Breakout Factor (Das, 1990).

The breakout factor, F_q is defined as the ratio between the uplift bearing pressure and the effective vertical stress at the upper helix level. The following expression can be used to estimate the breakout factor (Das and Seeley, 1975):

$$F_q = 1 + 2[1 + m(\frac{D_h}{D})](\frac{D_h}{D})K_U \tan\phi$$

where $(D_h/D) \le (D_h/D)_{cr}$ [6]

where m = coefficient dependant on soil friction angle

D_h = embedment depth to the top helix;

D = diameter of the upper helix

K_U = nominal uplift coefficient

ϕ = average frictional resistance angle for the soils above the upper helix

$(D_h/D)_{cr}$ = critical embedment ratio

The breakout factor, F_q depends on several parameters such as the embedment depth ratio (D_h/D), weight of soil above the helix, shape of helix, and angles of internal friction for the soils above the helix. Merrifield *et al* (2006) concluded that the circular shape of the helices provides higher resistance by about 20% compared to the square shape. It can be seen from Eqn. (5), that F_q increases with embedment ratio until the critical embedment ratio is reached, after which F_q is independent of embedment depth. The estimated critical embedment ratio, $(D_h/D)_{cr}$ for the compact to

very dense sand layer above the upper helix considered in the present study varied between 4.4 to 7.8.

The uplift capacities were estimated using Eqns. (2), (5) and (6) using soil parameters from Table 1. The estimated axial capacities for piles ST3 and ST21 are presented in Table 7. The estimated m and K_u values were 0.25 and 1.5 and the estimated breakout factor F_q using Eqn. (6) was 16. The estimated capacities were compared to the measured capacities based on the 5% criterion and a reasonable agreement was obtained between measured and estimated capacities. The measured capacity for ST21 was about 30% higher than the estimated value. A possible reason for that discrepancy is the presence of localized denser sand zone at the location of ST21 pile load test.

At test sites 2 and 3, the estimated m and K_u values were 0.27 and 1.67 and the estimated breakout factor F_q was 19. The estimated and measured capacities of piles ST25 and ST32 were in reasonable agreement.

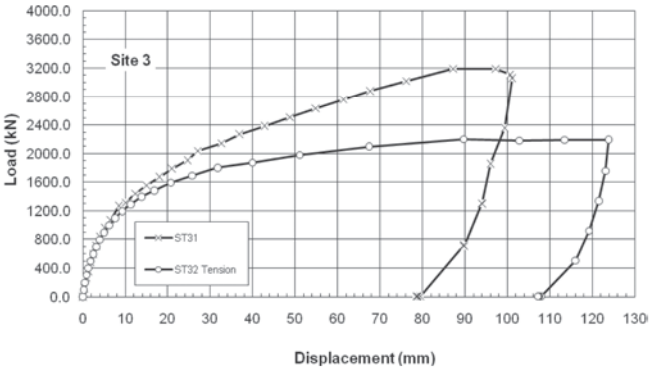

[FIG. 11] Comparison between Axial Compressive and Tensile Load Tests for Piles ST31 and ST32

Comparison between Compressive and Uplift Load Test Results

The results of both compressive and uplift load tests for piles ST31 and ST32 tested in cohesionless soil at test Site 3 are compared in Fig. 11. It should be noted that both piles were Type 8 with the same configuration and embedment depth of 5.0 m (16.4 ft). It can be seen from Fig. 11 that the load-displacement relationships were almost identical for both piles at the early stages of loading, up to displacement level of about 5 mm (0.2 in) which generally represented the elastic deflection of the pile, which in turn generally represents the shaft resistance. Therefore, the shaft friction under compression and uplift loading was similar. However, at higher displacement levels, when pile ST31 was tested in compression, it offered higher resistance when compared to when pile ST32 was tested in tension. Comparing between axial capacities of piles ST31 and ST32 (Tables 6 and 7) indicates that the compressive capacity of pile ST31 was about 19% higher than the uplift capacity of pile ST32. The lower end bearing resistance of the helical pile tested in tension is mainly due to the differences in the failure mechanism under tension and compression loading, combined with the smaller projected area of the upper surface of the bottom helix compared to the total area of lower surface of the bottom helix that includes the soil plug inside the pile shaft for piles tested in compression. Another comparison between piles tested in compression and tension can be made using the stiffness at the pile head defined as the slope of load-displacement curves. In general,

[TABLE 7] Comparison between Measured and Estimated Axial Tensile (Uplift) Capacities

Site	Test ID	Pile Type	Ultimate Capacity Estimated			Ultimate Capacity (5%) Measured			Prediction Ratio
			Shaft kN (kips)	Helix(es) kN (kips)	Total kN (kips)	Shaft kN (kips)	Helix(es) kN (kips)	Total kN (kips)	
Site 1	ST3	4	691 (155.3)	1278 (287.3)	1970 (442.6)	150 (33.7)	1843 (414.3)	1993 (448.0)	0.99
	ST21	5	350 (78.7)	690 (155.1)	1040 (233.8)	200 (45.0)	1297 (291.6)	1497 (336.6)	0.70
Site 2	ST25	8	1066 (239.6)	2182 (490.5)	3248 (730.1)	960 (215.8)	1940 (436.1)	2900 (651.9)	1.12
Site 3	ST32	8	544 (122.3)	1151 (258.8)	1695 (381.1)	500 (112.4)	1372 (308.4)	1872 (420.8)	0.91

at low displacements levels, both piles ST31 and ST32 showed similar stiffness. However at higher displacement levels (i.e. at displacements greater than 5 mm or 0.2 in) the stiffness of pile ST31, which was tested in compression, was higher than that of pile ST32 tested in tension.

Installation Torque – Pile Capacity Relationship

Empirical methods have been established for a relation between torque and ultimate pile capacity. It has been statistically analyzed based on a large database, and the method has been used successfully in the construction of many anchors over the past twenty years as indicated by Hoyt *et al.* (1995). The empirical relationship can be expressed as (Hoyt and Clemence, 1989; CFEM, 2006):

$$Q_t = K_t T \quad [7]$$

where K_t = empirical factor; and

T = average installation torque

It should be noted that torque-load correlations reported in the literature are established for small-diameter anchors resisting uplift loads. Therefore those correlations should be used with caution to estimate the uplift capacities of large diameter helical piles due to size effect and shape of the shaft (i.e. square or round shaft). Moreover, the torque exerted during pile installation is dependent on several factors such as soil strength parameters, groundwater levels, level of soil disturbance due to construction activity, pile configuration, helix shape, pitch size, vertical forces exerted on pile during installation, and frequency of calibrating the equipment.

As an example to some deviations that may occur during construction, at test site 1, pilot holes were predrilled to facilitate pile installation through frozen and hard soils. At test site 3, the leading edge of the helixes was trimmed to facilitate pile installation through cobbles. Therefore the torque-capacity relationship cannot be used with certainty in these cases. In addition to that, for dense sand soils encountered at sites 1 through 4, dilatation is expected to occur during installation which shows higher torque values during installation that do not necessarily represent the long-term soil conditions.

The torque-load correlation factor, K_t for compression and uplift loading found here for the reported study are also presented in Table 8. It can be seen from Table 8 that a ratio

[TABLE 8] Summary of Torque-Capacity Factors

	Test ID	Pile Type	Shaft Diameter mm (in)	No of Helixes	Installation Torque at end of installation kN.m (ft lb)	Embedment Depth m (ft)	Axial Capacity kN (kips)	K_t m^{-1} (ft^{-1})
Site 1	ST1	4	324 (12 ¾)	2	211.5 (156,000)	9.0 (29.5)	2030 (456.4)	9.6 (2.9)
	ST2	3	324 (12 ¾)	1	211.5 (156,000)	9.5 (31.2)	1892 (425.3)	8.9 (2.7)
	ST3	4	324 (12 ¾)	2	211.5 (156,000)	9.5 (31.2)	1993 (448.0)	9.4 (2.9)
	ST20	5	406 (16)	1	338.3 (250,000)	6.1 (20.0)	2533 (569.4)	7.5 (2.3)
	ST21	5	406(16)	1	338.3 (250,000)	5.7 (18.7)	1497 (336.5)	4.4 (1.3)
	ST22	7	508 (20)	1	338.3 (250,000)	5.75 (18.9)	2200 (494.5)	6.5 (2.0)
Site 2	ST24	8	406 (16)	2	338.0 (250,000)	5.95 (19.5)	2920 (656.4)	8.6 (2.6)
	ST25	8	406 (16)	2	338.0 (250,000)	9.71 (31.8)	2900 (651.9)	8.6 (2.6)
Site 3	ST31	8	406 (16)	2	338.0 (250,000)	5.0 (16.4)	2320 (521.6)	6.9 (2.1)
	ST32	8	406 (16)	2	338.0 (250,000)	5.0 (16.4)	1872 (420.8)	5.5 (1.7)
Site 4	ST41	8	406 (16)	2	326.0 (240,400)	10.5 (34.4)	2510 (564.2)	7.7 (2.3)

of torque to ultimate compressive capacities (using 5% criterion) for piles with single and double helixes varied between 9.6 m^{-1} (3 ft^{-1}) and 5.5 m^{-1} (1.7 ft^{-1}). The values of K_t for tension piles varied between 9.4 m^{-1} (2.9 ft^{-1}) and 4.4 m^{-1} (1.3 ft^{-1}). It should be noted that the assessed torque factors were generally lower than the suggested torque factor in CFEM (2006) of 3/ft (10/m) for shaft diameters approaching 200 mm (8 in). Moreover torque factors for piles with double helixes (i.e. type 2, 4 and 8) were higher than those with single helix (i.e. type 3, 5 and 7). Torque factors were relatively lower for piles ST31, ST32 and ST41 with trimmed helixes and were 6.9, 5.5 and 7.7, respectively. In addition to that, torque factors for piles tested in tension were lower than those measured in compression. This observation supported that the present empirical torque-capacity relationship is not adequate to estimate axial capacities of helical piles.

CONCLUSIONS

A full-scale pile load testing program was carried out using single and double-helix piles with different shaft and helix diameters, installed in dense to very dense sand, in order to investigate their axial performance under axial compressive and uplift loading conditions. The findings of this study can be summarized in the following conclusions:

1. Helical piles with relatively large diameters up to 508 mm (20 in) were successfully installed into dense to very dense soils.
2. The load-displacement curves of piles tested in compression and tension displayed typical trends including an initial linear segment, followed by a highly non-linear segment and then a near linear segment.
3. The creep effect assessed in the present study for dense to very dense sand was negligible. Therefore, it is suggested that the ASTM quick pile load test using Procedure A provides a reasonable means of estimating the axial capacities of helical piles installed in dense sand and presented in the current study.
4. The axial tensile (uplift) capacities of helical piles installed in dense to very dense sand varied between about 1500 kN and 2900 kN (337 kips and 652 kips). The tensile capacities of helical piles were about 80% of the compressive capacities.
5. The axial capacities of helical piles tested in cohessionless soils presented in this study may be estimated based on the bearing capacity theory using individual bearing method where, the ultimate axial capacity of the pile is the sum of individual bearing capacities of all helixes and shaft resistance. The major factors that affect the axial capacities are the pile geometry (diameter, depth and spacing of helixes), soil and groundwater profile, as well as the installation procedures.
6. If the predrilling process is used to facilitate installation of helical piles, a reduction of the shaft resistance is expected due to soil disturbance. In the present study skin friction was reduced by up to 50%. Depth of predrilling is another factor that affects the capacities of the individual helixes. Therefore depth of predrill should be considered by the pile designer to avoid under design helical piles.
7. A comparison between compression and uplift load test results suggested that similar shaft resistances were developed under compression and uplift load conditions. However, the end bearing component of uplift capacities of the helical piles were controlled by the soils above the helix.
8. Monitoring torque during installation can provide a qualitative measure for estimating the relative soil strength at location of installation. It is possible that a correlation between torque and soil strength may exist, however thorough investigation is required to establish this correlation. Nevertheless, monitoring torque during installation provides a viable method of assuring the quality of installation and confirming design assumptions.

ACKNOWLEDGEMENTS

The author would like to thank Almita Piling Inc., for allowing use of the test data and Imperial Oil for the opportunity to carry out the load testing program at their site. The author would like to thank Ms. Kimberly Steward of Imperial Oil, Mr. Chris Palanque of FLUOR Canada Ltd. and Almita field staff for their patience, attention to details, as well as their careful installation and load testing methods for piles considered in this study. In particular the author would like to thank Messrs, Mathew Young and Scott Blackie.

REFERENCES

1. ASTM D 1143/D 1143M – 07. 2007. Standard test methods for deep foundations under static axial compressive load. Annual Book of ASTM Standards
2. ASTM D 3689-07. 2007. Standard Test Methods for Deep Foundations under Static Axial Tensile Load. Annual Book of ASTM Standards
3. Bobbitt, D.E. and Clemence, S.P. 1987. Helical Anchors: Application and Design Criteria, Proceedings of the 9th Southeast Asian Geotechnical Conference, Bangkok, Thailand: 6-105 to 6-120
4. CFEM. 2006. Canadian Foundation Engineering Manual. 4th Edition. Canadian Geotechnical Society, Technical Committee on Foundations, BiTech Publishers Ltd., Richmond, BC
5. Das, B.M. 1990. Earth anchors. Elsevier, Amsterdam
6. Das, B.M. and Seeley G. R. 1975. Breakout resistance of horizontal anchors. Journal of Geotechnical Engineering Division, ASCE, 101(9): 999–1003
7. Davisson, M.T. 1972. High capacity piles. *Proceedings Lecture Series on Innovations in Foundation Construction*, Soil Mechanics Division Illinois Section. ASCE, Chicago, pp 81 -112
8. Davisson, M.T. 1993. Negative skin friction in piles and design decisions. *Proceedings 3rd International Conference Case Histories in Geotechnical Engineering* (3), St Louis, pp 1793 -1801
9. IBC. 2009. International Building Code. 1st Print. International Code Council, Inc.
10. Hoyt, R.M., and Clemence, S.P. 1989. Uplift capacity of helical anchors in soil, *Proceedings of the 12th International Conference on Soil Mechanics and Foundation Engineering*, Rio de Janerio, Brazil, Vol. 2, pp. 1019-1022
11. Hoyt, R., Seider, G., Reese, L. C., and Wang, S. T. (1995). Buckling of helical anchors used for underpinning: Foundation upgrading and repair for infrastructure improvement. Edited by William F. K. and Thaney, J. M. Geotechnical Special Publication No. 50, ASCE, pp. 89-108
12. Kulhawy, F.H. and Hirany, A. 1989. Interpretation of load tests on drilled shafts; Part 2: Axial uplift, *Proceedings of Foundation Engineering: Current Principles and Practices*, ASCE, Vol. 2, pp. 1150-1159
13. Kulhawy, F.H. and Hirany, A. 2009. Interpreted failure load for drilled shafts via Davisson and L1-L2, *Proceedings of the 2009 International Foundation Congress and Equipment Exposition*, Orlando, Florida, GSP No. 185, pp. 127-134
14. Kurian, N. P. and Shah, S. J. 2009. Studies on the behaviour of screw piles by the finite element method. Canadian Geotechnical Journal, 46: 627– 638
15. Lade, P.V... and Duncan, J.M. 1975. Elasto-plastic stress strain theory for cohesion less soil. Journal Soil Mechanics and Foundation Division, ASCE, 101(10): 1037–1053
16. Merifield R.S., Lyamin A.V., Sloan S.W. 2006. Three-dimensional lower bound solutions for the stability of plate anchors in sand. Géotechnique, 56(2): 123-132
17. Meyerhof, G.G., and Adams, J.I. 1968. The Ultimate uplift capacity of foundations. Canadian Geotechnical Journal, V(4): 225–244
18. Mitsch, M.P., and Clemence, S.P. 1985. The Uplift capacity of helix anchors in sand. Uplift behavior of anchor foundations in soil. In *Proceedings of ASCE, New York, N.Y.*, pp. 26-47
19. NeSmith, M.W., and Siegal, T.C. 2009. Shortcomings of the Davisson Offset Limit Applied to Axial Compressive Load Tests on Cast-in-Place Piles, *Proceedings of the 2009 International Foundation Congress and Equipment Exposition*, Orlando, Florida, GSP No. 185, pp. 568-574
20. Perko, H. A. 2009. Helical Piles: A Practical Guide to Design and Installation. John Wiley & Sons. New York, N.Y.
21. Sakai, T. and Tanaka, T. 1998. Scale effects of a shallow circular anchor in dense sand. Soils Foundations, 38(2): 93- 99
22. Sakr, M. 2009. Axial and lateral behaviour of helical piles in oil sand. Canadian Geotechnical Journal, 46(9): 1046-1061
23. Sakr, M., Mitchells, R., and Kenzie, J. 2009. "Pile load testing of helical piles and driven steel piles in Anchorage, Alaska. Submitted

to DFI 34th Annual Conference On Deep Foundations, October 21 – 23, 2009, Kansas City, Missouri, USA

24. Tagaya, K., Tanaka, A. and Aboshi, H. 1983. Application of finite element method to pullout resistance of buried anchor. Soils Foundations, 23(3): 91-104

25. Tagaya, K., Scott, R.F. and Aboshi, H. 1988. Pullout resistance of buried anchors in sand. Soils Foundations, 28(3): 14-130

26. Vesic, A.S. 1971. Breakout resistance of objects embedded in ocean bottom. Journal of Soil Mechanics and Foundation Division, ASCE, 97(SM 9): 1183–1205

27. Zhang, D.J.W. 1999. Predicting capacity of helical screw piles in Alberta soils. MSc. Thesis, The University of Alberta, Edmonton, Alberta, Canada